






Evaluation of secondary electron intensities for dopant profiling in ion implanted semiconductors: a correlative study combining SE, SIMS and ECV methods

C N Shyam Kumar¹ , Saba Tabean^{1,2} , Audrey Morisset³, Philippe Wyss³, Mario Lehmann³ , Franz-Josef Haug³, Quentin Jeangros³, Aïcha Hessler-Wyser³ , Nathalie Valle⁴, Tom Wirtz¹ and Santhana Eswara^{1,*} 

¹ Materials Research and Technology Department, Advanced Instrumentation for Nano-Analytics (AINA), Luxembourg Institute of Science and Technology (LIST), 41, Rue Du Brill, Belvaux L-4422, Luxembourg

² University of Luxembourg, 2 Avenue de l'Université, Esch-sur-Alzette L-4365, Luxembourg

³ Ecole Polytechnique Fédérale de Lausanne (EPFL), Institute of Microengineering (IMT), Photovoltaics and Thin Film Electronics Laboratory, Rue de La Maladière 71b, 2002 Neuchâtel, Switzerland

⁴ Advanced Characterization Platform (ACP), Luxembourg Institute of Science and Technology (LIST), Materials Research and Technology Department, 41, Rue Du Brill, L-4422 Belvaux, Luxembourg

E-mail: santhana.eswara@list.lu

Received 1 March 2021, revised 18 May 2021

Accepted for publication 4 June 2021

Published 29 June 2021



Abstract

This study evaluates the secondary electron (SE) dopant contrast in scanning electron microscopy (SEM) and helium ion microscopy (HIM) on boron implanted silicon sample. Complementary techniques like secondary ion mass spectrometry and electrochemical capacitance voltage (ECV) measurements are used to understand the dopant profile and active dopant distribution before and after a thermal firing, a step carried out to remove implantation damage and to electrically activate the implanted boron. Thermal firing resulted in an activation efficiency of 33%. HIM showed higher contrast than SEM having more defined peak with a lower background contribution. Variations in dopant concentration near the peak maximum were observed in ECV measurements, which was not observed in the intensity profiles from both SEM and HIM. This study demonstrates the effectiveness of SE dopant profiling as a quick tool to map the electrically active dopant concentrations even in far-from-equilibrium materials such as ion implanted samples.

Keywords: dopant profiling, helium ion microscopy, secondary electrons, secondary ion mass spectrometry, electrochemical capacitance-voltage

(Some figures may appear in colour only in the online journal)

* Author to whom any correspondence should be addressed.



Original content from this work may be used under the terms of the [Creative Commons Attribution 4.0 licence](https://creativecommons.org/licenses/by/4.0/). Any further distribution of this work must maintain attribution to the author(s) and the title of the work, journal citation and DOI.

1. Introduction

There has been a growing interest in semiconductor industry for fast and reliable characterization of dopant concentration at high spatial resolution. Secondary electron (SE) imaging offers a reliable and quick characterization method for dopant profiling [1–5]. The dopant contrast arises from the local variations in the electronic structure of the near surface region, which affects the SE yield. It has been experimentally and theoretically proven that p regions appear brighter in the images while the n regions appear darker, owing to their higher and lower SE yield, respectively [4, 6]. Thus, doping contrast provides a rapid 2D nanoscale imaging method and emerged as a promising alternative among various techniques used in the industry.

The emergence of helium ion microscopy (HIM) has further improved the spatial resolution and sensitivity of dopant profiling using SE imaging [7–11]. HIM produces a smaller spot size owing to the atomically sharp ion source and lower de Broglie wavelength (due to the heavier ion mass). Moreover, the SE yield in HIM is highly localized due to the lower interaction volume in the near-surface region of the sample, i.e. in the region where SEs are emitted from. This improves the spatial resolution in HIM compared to scanning electron microscopy (SEM) [10, 11]. It was also shown that the SE emission in HIM is more sensitive to the surface electronic variations compared to SEM, which makes HIM more suitable compared to SEM for dopant profiling with improved sensitivity and spatial resolution [12].

The semiconductor industry uses various techniques to incorporate dopants into semiconductors. One widely used technique is ion implantation. The major issue concerning this technique is the implantation damage caused during the process [13]. The damage induces amorphization and defects in the lattice. The incorporated dopant will not occupy the electrically active substitutional sites but rather pins to defects and vacancies, making it electrically inactive. After the implantation, an annealing process is necessary to incorporate the dopants into the active substitutional sites [14]. The characterization of the active dopant concentration is of vital importance to correlate to the properties and performance of the sample. Secondary ion mass spectrometry (SIMS) is a widely used high sensitivity technique for dopant profiling in semiconductor industry. Recent developments in correlative characterization methods have improved the resolution of SIMS imaging [7, 15, 16]. There is also a continuing effort in developing correlative methods for dopant profiling with high sensitivity and high spatial resolution, as well as for the precise quantification of SIMS intensities [17–19]. However, the SIMS technique requires calibration with reference samples to determine the dopant concentration and even then it gives only the total dopant concentration and cannot distinguish the active and inactive dopants in the matrix. On the other hand, techniques like electrochemical capacitance voltage (ECV) can provide depth profiles of the electrically active dopant concentrations, however determination of the etching depth is not straightforward and thus requires precise measurement of etching depths [20]. Both techniques have the limitation that

the sample volume is consumed during the analysis which is not the case for dopant profiling based on SE imaging. Since the SE contrast is directly related to the local electronic structure, which is governed by the active dopant concentration, SE imaging provides a rapid noncontact method to map electrically active dopant concentration in a matrix.

There are previous works comparing the dopant contrast from SEM and HIM, but most of them are carried out on layered samples grown with known dopant concentrations [1–3, 21, 22]. On the other hand, ion implanted samples show a continuous variation of concentration and can have vacancy/dopant clustering, which induces local variations in doping. Thus, SE intensity dopant profiling in ion implanted samples requires a more detailed examination. In this study we investigated the dopant contrast of electrically active dopant in boron implanted silicon samples using SEM and HIM and compare it with SIMS and ECV profiles. Boron-implanted silicon samples were heat treated to decrease the implantation damage and activate the boron. SIMS measurements were carried out to assess the dopant profiles before and after firing. ECV measurements were carried out to obtain depth profiles of the electrically active boron before and after firing, and they were correlated with the SE contrast obtained from SEM and HIM. The present approach helps to understand the SE dopant contrast from SEM and HIM in the boron implanted samples and can be extended to other material systems as well.

2. Materials and methods

Boron implantation was carried out on a silicon wafer with a crystal orientation $\langle 100 \rangle$ at the Surrey Ion Beam Centre, Guildford, UK. The Si wafer substrate (Virginia Semiconductor Inc. USA) used for the implantation was an n-type with phosphorous dopant atoms with a concentration $\sim 1 \times 10^{15}$ at. cm^{-3} . Implantation energy was 190 keV with a total dose of 10^{16} ions cm^{-2} . The high energy of implantation makes sure that the concentration maximum forms as deep as possible (550 nm in the present study) from the surface and gives an extended concentration profile. Further details of the implantation conditions are given elsewhere [18]. The concentration profile as a function of depth was estimated using the Monte Carlo based simulation program SRIM (version 2013) [23], showing the maximum concentration of B to be 5×10^{20} at. cm^{-3} (or 1 at. %) at a depth of 550 nm from the surface. Firing of the implanted samples was carried out in a vacuum furnace at 700 °C for 15 s, followed by cool-down in the furnace until room temperature. The temperature and the time were selected to lower implantation damages and activate boron dopants without causing significant diffusion of the implanted boron.

SIMS depth profiling was carried out on a CAMECA SC Ultra using O_2^+ primary ions with an impact energy of 1 keV. The primary beam current was 10 nA. The scanned area was $200 \times 200 \mu\text{m}^2$ and the analyzed area was $63 \mu\text{m}$ in diameter. $^{30}\text{Si}^+$ and $^{11}\text{B}^+$ ions were collected and analyzed. Standard procedure was used to convert secondary ion counts to concentration by relating the known implantation dose

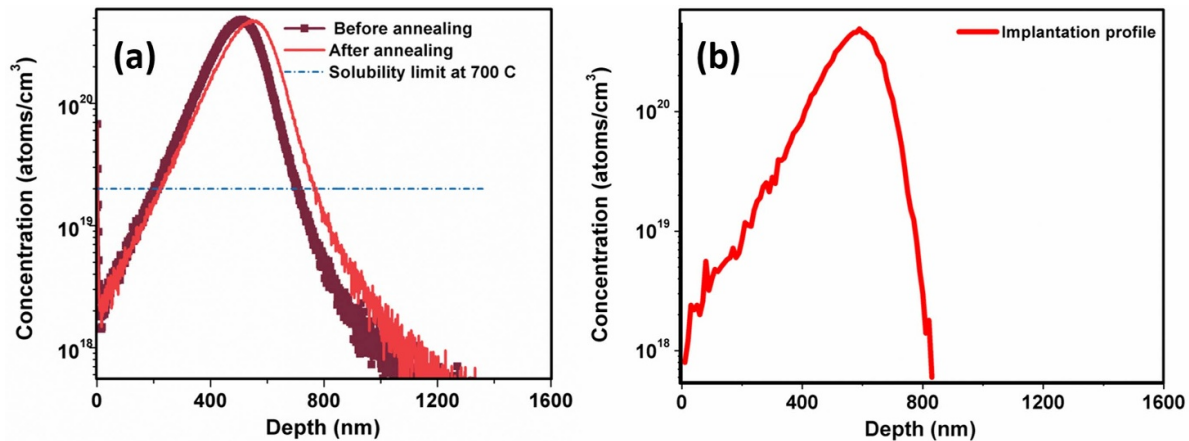


Figure 1. (a) SIMS depth profile of boron-implanted silicon sample before and after firing to 700 °C. (b) the implantation profile obtained from the SRIM calculation. The dotted blue line in (a) shows the solubility limit of boron in silicon (2×10^{19} atoms cm^{-3}) at 700 °C [25, 26].

(10^{16} ions cm^{-2}) to the integrated B signal over the depth of implantation [24]. The SIMS sputtering time was converted to depth, assuming a linear erosion after measuring the crater depth at the end of the experiment using a KLA-Tencor P17 profilometer.

SE imaging was carried out on cross-sections in a Hitachi SU-70 SEM. The samples were freshly cleaved to minimize the oxidation effects. Imaging was carried out using standard imaging condition. Acceleration voltage used was of 2 kV with a probe current of 3.2 μA . The scan area is 640×480 pixels. HIM analysis was carried out under high vacuum in a HIM from Carl Zeiss. Acceleration voltage was 25 kV with probe current ranging from 5.2 to 4.8 pA. The scan area was 1024×1024 pixels with a step size of 3.9 nm and a dwell time of 80 μs .

ECV measurements were carried out using an ECV CVP21 tool from WEP with a 0.1 mol l^{-1} NH_4F solution as etchant. The measurements were performed on cleaved pieces of samples of approximately 2×2 cm^2 .

3. Results and discussion

3.1. SIMS depth profiling

Figure 1 shows the SIMS depth profile before and after thermal firing and the implantation profile obtained from the SRIM calculation. Despite the fact that SRIM calculation assumes the Si to be amorphous, the SIMS peak position matches well with the implantation profile obtained from the SRIM calculation. The tail seen in the SIMS profile between 800 to 1200 nm is not observed in the simulated implantation profile. This can be attributed to ion mixing resulting from primary ion bombardment during SIMS analysis. The dotted blue line shows the solubility limit of boron in silicon (2×10^{19} atoms cm^{-3}) at 700 °C [25, 26]. The peak concentration of boron is much higher than the solubility limit, which may lead to precipitation and clustering of boron. From the SIMS data, we can observe that the dopant profiles are similar with a slight shift in the peak after firing. The full width at half maximum showed a value

of 190 and 205 nm before and after firing respectively. The firing step after the implantation is however known to induce transient enhanced diffusion. During implantation, vacancies are created, and vacancy clustering happens. These vacancies can facilitate diffusion of implanted boron during thermal treatment. This results in abnormal diffusion in some of the implanted boron atoms while the others will be trapped as boron clusters and will be electrically inactive [13, 14]. From the shape of the boron peak we can conclude that the thermal firing has not created any significant diffusion of boron, mainly because of the rapid heating rate and short holding time. The shift in the peak after firing can originate from the crystallisation of the silicon matrix, affecting the erosion rate [27]. Indeed, the dose used (10^{16} ions cm^{-2}) for the implantation is high enough to cause amorphization of the silicon lattice [13], that can then crystallize during rapid annealing. This difference in the crystallinity can cause difference in the sputtering rate in SIMS and shift in the peak.

3.1.1. Activation of boron by firing. The SIMS analysis shows that the implanted boron reaches a peak concentration of 4.8×10^{20} atoms cm^{-3} . The SIMS profiles correspond to the total dopant concentration and it cannot distinguish active and inactive boron atoms. Due to the implantation damage, boron atoms can be trapped in vacancies and interstitials, preventing them to go into the electrically active substitutional sites. The rapid annealing can heal the implantation defects so that boron can go to the active substitutional sites. While the SIMS analysis can only give the total dopant concentration, the ECV measurements can approximate the electrically active dopant concentration. Before firing there is no indication of any p-type doping in the sample, indicating that the implanted boron is not active in the n-type silicon substrate as seen in the figure 2. It should be noted that the ECV profiling in amorphous materials is not well understood and hence the interpretation of the ECV profile of the as-implanted sample is not straightforward. However, after firing, the amorphous areas are crystallized and the ECV profiles can be interpreted. The profile after firing shows an increasing p-type doping around a depth of 600 nm,

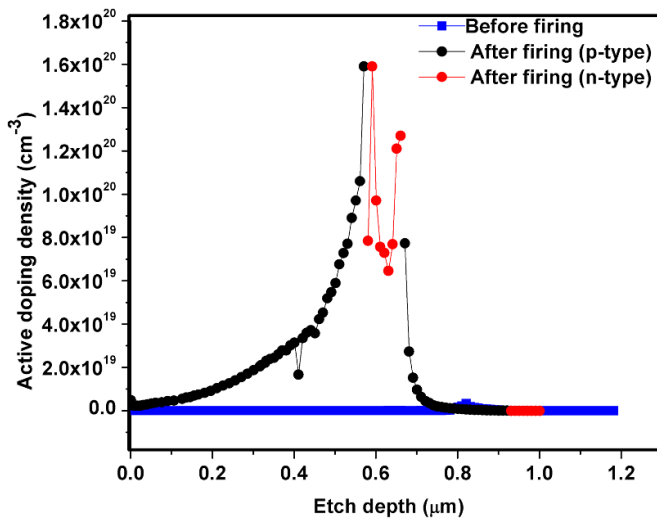


Figure 2. ECV profiles of boron implanted silicon sample before and after heat treatment to 700 °C.

which coincides well with the SIMS profile and the simulated implantation profile. The maximum active dopant concentration was found to be $1.59 \times 10^{20} \text{ atoms cm}^{-3}$. This accounts for a 33% activation efficiency which shows the effectiveness of firing on the activation of the implanted boron. There is some n-type doping at the peak of the profile (indicated by red dots). This difference in doping can arise from the local inhomogeneities due to the clustering of boron during implantation and/or firing. Previous reports show local precipitation of boron when the implantation exceeds the solubility limit of boron [13, 14]. This kind of local variation can cause boron rich and deficient areas resulting in variation of doping.

3.2. Effect of firing on the SE yield

The SEM and HIM images and the contrast profiles from the implanted and fired sample cross-sections are shown in figure 3. The contrast percentage is calculated using the formula $(I - I_b) / (I + I_b) \times 100$, where I is the measured intensity and I_b is the average background intensity measured laterally over a range of 500 nm starting from a region 1 μm away from the edge. This calculation helps to normalize the intensities independent of the contrast and brightness settings of the microscopes. Figures 3(a) and (b) show the SE images obtained in the SEM and contrast profiles of the implanted sample before and after firing. Before firing, the boron intensity was absent in most of the cleaved surfaces and showed a light, diffuse contrast in some regions. This might be arising from amorphization in the region and the resulting difference in work function than in the crystalline silicon [9, 28] and possibly from small amounts of the active boron.

On the contrary, the sample after firing shows a clear contrast from the active boron. The contrast of 15% in figure 3(a) is slightly higher than in the fired sample shown in figure 3(b). This is an anomaly that is attributed to the diffuse, broad, low-intensity peak and noisy signal in figure 3(a). It is still provided for the sake of completeness. However, visually, it is clear that figure 3(b) has higher contrast than figure 3(a). The peak

in the intensity profile in figure 3(b) coincides well with the SIMS and ECV profile and this clearly demonstrate that the intensity is arising from the active boron. Crystallization of the matrix after firing eliminates the contrast contribution from the amorphous region and the contrast can be attributed solely to the active boron. Similar trend can be observed from the SE intensity arising from the HIM measurements. From the contrast percentage calculation, we can observe that the HIM shows higher contrast compared to SEM.

A comparison of the normalized SE intensities from SEM and HIM of the fired sample is shown in figure 4. The normalized intensity plots are aligned with respect to the maximum intensity. This is to correct for the misalignment in the intensity plots occurring due to a slight tilting of the sample while loading in the SEM and HIM. The correction is minimum, and this will not significantly influence the observed FWHM of the profiles. The SEM intensity profile is narrow with high background contribution while the HIM intensity profile shows a well-defined peak until it reaches a stable background towards the right side of the peak. The broader peak width at the base of the peak in the HIM profile is not because of poorer lateral resolution, but points towards a lower (i.e. better) detection limit in HIM compared to the SEM. Comparing the SE emission, HIM produces a narrower spot size and has a lower scattering radius in comparison to electron beam of same energy. This results in narrower interaction volumes near the surface and thus more localized SE emission [29]. In the case of SEM, the dopant contrast is only visible with lower acceleration voltages. This is mainly because of the lower interaction volume and lower signal to noise ratio. On the other hand, HIM will have narrower interaction volumes near the surface (from where SE escape) and more localized SE emission even at higher accelerating voltages [30]. Hence different primary energies were chosen. Moreover, as He backscattering is very low compared to electrons, the SE in HIM is almost exclusively produced by the primary beam in HIM and contains more information about the near surface variations. On the other hand, even at an accelerating voltage as low as 2 kV, the SE contrast from SEM will have contribution from a larger SE emission area compared to HIM at 25 kV [30]. There will be also larger number of SE_{HS} (type 2 SE) generated from the back scattered electrons which contribute to the image formation in SEM [31]. These effects can lead to higher background contribution in SEM compared to HIM and can affect the detection limit in SEM. This is consistent with previous studies on samples grown by chemical vapor deposition which showed higher detection limit for HIM compared to SEM [10, 11].

Now it is important to compare the ECV profile and the SE intensity profiles from SEM and HIM. As shown previously, the ECV profile shows changes in dopant concentration near the higher concentration range. Both intensity profiles are smooth and continuous compared to the fluctuations observed in the ECV profile. There is a dip in the SE intensity profile around 300 nm just before the onset of the SE intensity peak (indicated by blue arrow on figure 4), which is absent in SIMS and ECV measurements and thus cannot be originating from the difference in dopant concentration.

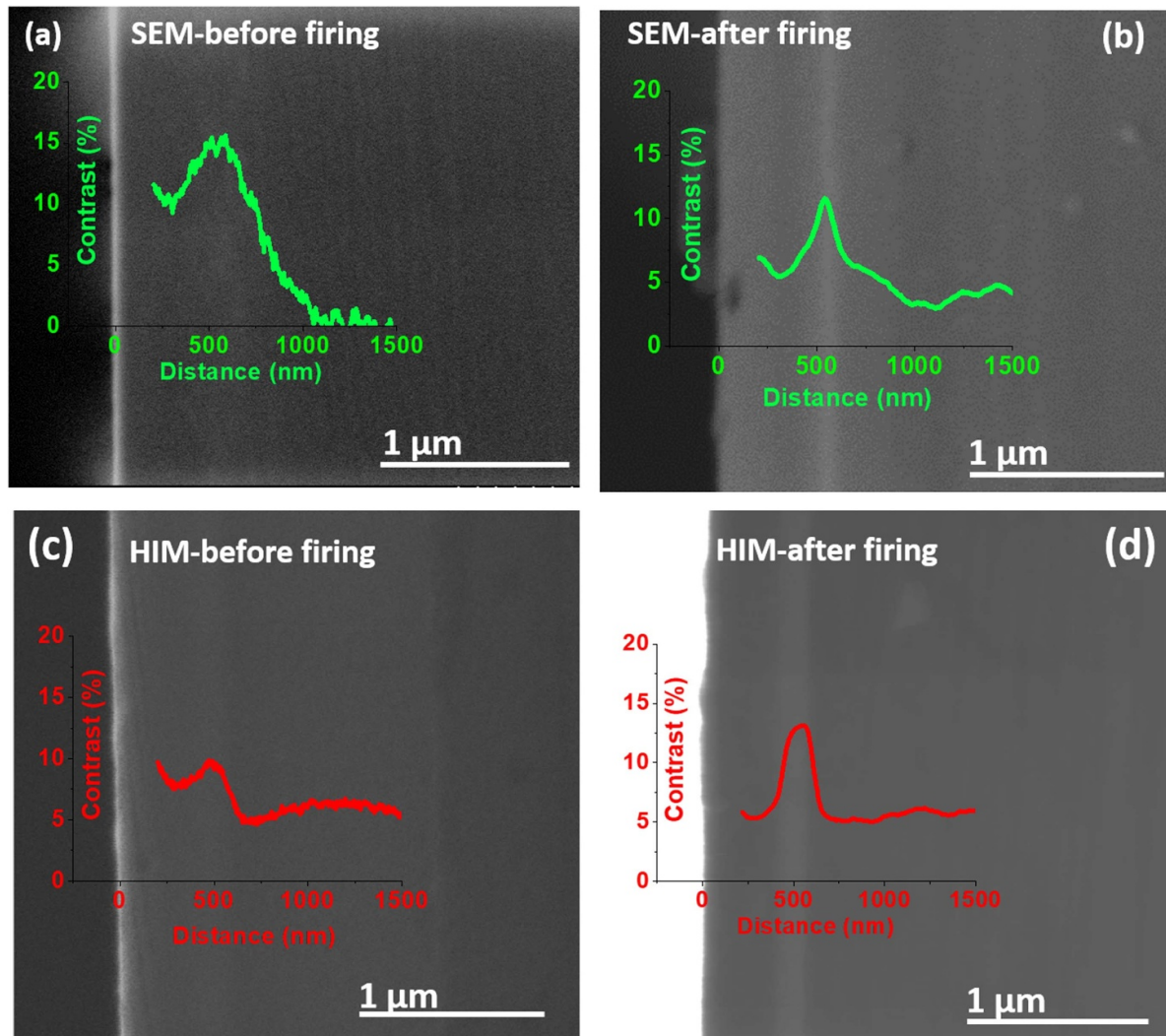


Figure 3. Comparison of cross-sectional SE images and the contrast profiles obtained by SEM (a), (b) and HIM (c), (d) from the implanted sample before and after firing. The SE intensities were column averaged over 480 and 1024 pixels for SEM and HIM respectively. Intensity profile until 200 nm from the edge is not shown in the image. This is to avoid the high intensities arising from the edge contrast.

The ECV measurement is based on the establishment of a semiconductor–electrolyte Schottky contact to create a depletion region at the surface of the sample. The determination of carrier concentration is done by measuring the differential capacitance of the Schottky barrier produced at the semiconductor–electrolyte interface [20, 32]. The ECV measurement offers high sensitivity and high detection range owing to its direct measurement of charge carrier concentration [33, 34].

On the other hand, SE intensity profiling relies on the local SE yield, which is related to the variation of the work function with doping [2, 11]. The contrast between differently doped regions is diminished by surface states of a terminated crystal as bands will bend downwards at the surface for p-type doping and upwards for n-type doping. Thus, for weak doping the SE contrast can be completely removed by pinning to a single Fermi-level, whereas it may remain noticeable when the doping is high enough to saturate the surface states [2]. Now looking at the dip in the intensity profile, previous work

on photoemission thresholds [35] in doped silicon has shown that the Fermi-level of a freshly cleaved sample is essentially pinned by the surface states, resulting in an almost constant work-function that is virtually independent of the underlying doping type and concentration. Hence, the dip in the SE intensity cannot be explained from the band bending at the surface. Instead, it might be attributed to the extent of the depletion region in the bulk and its convolution with the SE escape depth.

Though the SEM and HIM images have higher resolution, the dopant profiling is fundamentally restricted by the surface potential caused by the surface band bending [2, 4]. Thus, small local variations in the dopant depth profile, which can be detected by the ECV, might not be visible in an SE intensity profile. Furthermore, the SE intensity profiles are smoothed by the volume from which SE emission occurs. It should be also noted that in the commercial SEM and HIM, the SE intensity is scaled over values between 0 and 255 (8 bit images), which can further smooth out subtle local intensity variations in addition to a loss of dynamic range. These observed effects

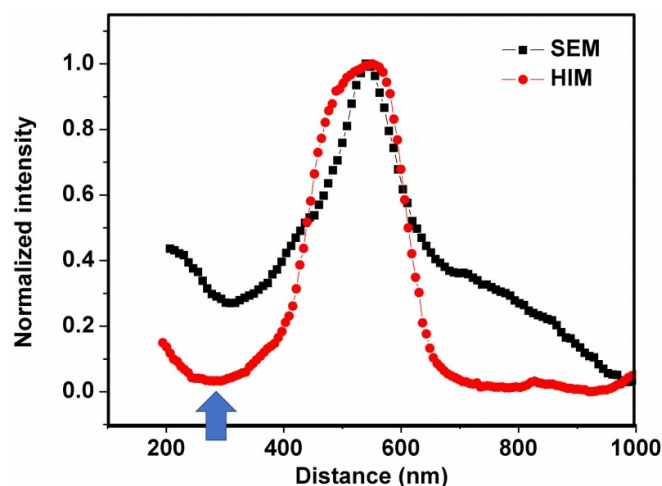


Figure 4. Normalized SEM and HIM SE intensity profiles after firing.

necessitate extra care and the need of complementary characterization techniques for the better understanding of SE intensity profiles in ion implanted samples.

4. Conclusion

The SE contrast of electrically active dopant in boron implanted silicon samples has been studied using SEM and HIM and correlated with SIMS and ECV profiles. The as-implanted sample showed only low diffuse SE contrast due to the electrically inactive nature of the dopant which is corroborated by ECV measurements. Thermal firing at 700 °C for 15 s was carried out to cure the implantation damage and activate the dopants. SIMS measurements confirmed that no significant diffusion of boron occurred because of the firing, while the ECV profiling showed an increasing p-type doping with maximum active dopant concentration at 1.59×10^{20} atoms cm⁻³, which accounts for a 33% activation efficiency. SE images after firing showed a clear contrast from the active boron distribution with HIM presenting a higher contrast compared to SEM, as can be seen by more defined peak with lesser background contribution. Variations in dopant concentration near the peak visible in the ECV measurements, were not observed in the intensity profiles from both SEM and HIM. This study shows the effectiveness of SE dopant profiling as a quick tool to obtain 2D maps of the electrically active dopants in ion implanted samples. This is advantageous over the 1D information provided by depth profiling using SIMS or ECV. However, when local dopant concentrations exceed the solubility limit, SE imaging is inadequate and complementary techniques like SIMS and ECV are necessary to obtain a complete understanding of the doping characteristics.

Data availability statement

The data that support the findings of this study are available upon reasonable request from the authors.

Acknowledgments

Authors would like to thank Brahime El Adib for his valuable help for carrying out SIMS analysis. This work was funded by the Luxembourg National Research Fund (FNR) by the grants INTER/SNF/16/11536628 (NACHOS) and PRIDE17/12246511/PACE. The work was co-funded by the Swiss National Science Foundation (SNF), Switzerland, under Grant No. 200021L_172924/1.

ORCID iDs

C N Shyam Kumar <https://orcid.org/0000-0003-4860-5327>
 Saba Tabean <https://orcid.org/0000-0002-1397-2154>
 Mario Lehmann <https://orcid.org/0000-0003-4325-306X>
 Aïcha Hessler-Wyser <https://orcid.org/0000-0003-1159-4193>
 Santhana Eswara <https://orcid.org/0000-0003-4151-2304>

References

- [1] Turan R, Perovic D D and Houghton D C 1996 Mapping electrically active dopant profiles by field-emission scanning electron microscopy *Appl. Phys. Lett.* **69** 1593–5
- [2] Sealy C P, Castell M R and Wilshaw P R 2000 Mechanism for secondary electron dopant contrast in the SEM *J. Electron Microsc.* **49** 311–21
- [3] Müllerová I, El-Gomati M M and Frank L 2002 Imaging of the boron doping in silicon using low energy SEM *Ultramicroscopy* **93** 223–43
- [4] El-Gomati M, Zaggout F, Jayacody H, Tear S and Wilson K 2005 Why is it possible to detect doped regions of semiconductors in low voltage SEM: a review and update *Surf. Interface Anal.* **37** 901–11
- [5] Buzzo M, Ciappa M, Stangoni M and Fichtner W 2005 Two-dimensional dopant profiling and imaging of 4H silicon carbide devices by secondary electron potential contrast *Microelectron. Reliab.* **45** 1499–504
- [6] Chee A K W, Broom R F, Humphreys C J and Bosch E G T 2011 A quantitative model for doping contrast in the scanning electron microscope using calculated potential distributions and Monte Carlo simulations *J. Appl. Phys.* **109** 013109
- [7] Wirtz T, De Castro O, Audinot J-N and Philipp P 2019 Imaging and analytics on the helium ion microscope *Annu. Rev. Anal. Chem.* **12** 523–43
- [8] Jepson M, Liu X, Bell D, Ferranti D, Inkson B and Rodenburg C 2011 Resolution limits of secondary electron dopant contrast in helium ion and scanning electron microscopy *Microsc. Microanal.* **17** 637–42
- [9] O'Connell R, Chen Y, Zhang H, Zhou Y, Fox D, Maguire P, Wang J J and Rodenburg C 2017 Comparative study of image contrast in scanning electron microscope and helium ion microscope *J. Microsc.* **268** 313–20
- [10] Chee A K W and Boden S A 2016 Dopant profiling based on scanning electron and helium ion microscopy *Ultramicroscopy* **161** 51–8
- [11] Chee A K W 2019 Principles of high-resolution dopant profiling in the scanning helium ion microscope, image widths, and surface band bending *IEEE Trans. Electron Devices* **66** 4883–7
- [12] Ward B W, Nott J A and Economou N P 2006 Helium ion microscope: a new tool for nanoscale microscopy and metrology *J. Vac. Sci. Technol. B* **24** 2871

- [13] Michel A E, Rausch W and Ronsheim P A 1987 Implantation damage and the anomalous transient diffusion of ion-implanted boron *Appl. Phys. Lett.* **51** 487–9
- [14] Landi E, Armigliato A, Solmi S, Kögler R and Wieser E 1988 Electrical activation of boron-implanted silicon during rapid thermal annealing *Appl. Phys. A Solids Surf.* **47** 359–66
- [15] Wirtz T, Philipp P, Audinot J-N, Dowsett D and Eswara S 2015 High-resolution high-sensitivity elemental imaging by secondary ion mass spectrometry: from traditional 2D and 3D imaging to correlative microscopy *Nanotechnology* **26** 434001
- [16] Vollnhals F, Audinot J-N, Wirtz T, Mercier-Bonin M, Fourquaux I, Schroepel B, Kraushaar U, Lev-Ram V, Ellisman M H and Eswara S 2017 Correlative microscopy combining secondary ion mass spectrometry and electron microscopy: comparison of intensity–Hue–saturation and Laplacian pyramid methods for image fusion *Anal. Chem.* **89** 10702–10
- [17] Di Russo E et al 2020 Multi-microscopy nanoscale characterization of the doping profile in a hybrid Mg/Ge-doped tunnel junction *Nanotechnology* **31** 465706
- [18] Eswara S et al 2019 A method for quantitative nanoscale imaging of dopant distributions using secondary ion mass spectrometry: an application example in silicon photovoltaics *MRS Commun.* **9** 916–23
- [19] Yedra L, Shyam Kumar C N, Pshenova A, Lentzen E, Philipp P, Wirtz T and Eswara S 2021 A correlative method to quantitatively image trace concentrations of elements by combined SIMS-EDX analysis *J. Anal. At. Spectrom.* **36** 56–63
- [20] Peiner E, Schlachetzki A and Krüger D 1995 Doping profile analysis in Si by electrochemical capacitance-voltage measurements *J. Electrochem. Soc.* **142** 576–80
- [21] Hyun M S, Hyun H Y, Yang J M, Kwak N Y, Kim W and Kim H J 2011 Practical application of 2D dopant profiling by LV-SEM *18th IEEE Int. Symp. on the Physical and Failure Analysis of Integrated Circuits (IPFA)* (IEEE) pp 1–3
- [22] Frank L, Hovorka M, El-Gomati M M, Müllerová I, Mika F and Mikmeková E 2020 Acquisition of the dopant contrast in semiconductors with slow electrons *J. Electron Spectros. Relat. Phenom.* **241** 146836
- [23] Mutzke A, Schneider R, Eckstein W and Dohmen R 2011 SDTrimSP version
- [24] Wilson R G, Stevie F A and Magee C W 1989 *Secondary Ion Mass Spectrometry: A Practical Handbook for Depth Profiling and Bulk Impurity Analysis* (New York: Wiley)
- [25] Garben B, Orr-Arienzo W A and Lever R F 1986 Investigation of boron diffusion from polycrystalline silicon *J. Electrochem. Soc.* **133** 2152–6
- [26] Vick G L and Whittle K M 1969 Solid solubility and diffusion coefficients of boron in silicon *J. Electrochem. Soc.* **116** 1142
- [27] Tomita M, Tanaka H, Kioke M and Takeno S 2005 Depth resolution parameters and sputtering rates extracted from amorphous and crystalline silicon materials for SIMS shallow depth profiling *J. Surf. Anal.* **12** 161–5
- [28] Ukah C I, Kruzelecky R V, Racansky D, Zukotynski S and Perez J M 1988 *In situ* work function measurements in evaporated amorphous silicon *J. Non. Cryst. Solids* **103** 131–6
- [29] Inai K, Ohya K and Ishitani T 2007 Simulation study on image contrast and spatial resolution in helium ion microscope *J. Electron Microsc.* **56** 163–9
- [30] Notte J, Ward B, Economou N, Hill R, Percival R, Farkas L and McVey S 2007 An introduction to the helium ion microscope *AIP Conf. Proc.* **931** 489–96
- [31] Bernstein G H, Carter A D and Joy D C 2013 Do SE II electrons really degrade SEM image quality? *Scanning* **35** 1–6
- [32] Blood P 1986 Capacitance-voltage profiling and the characterisation of III-V semiconductors using electrolyte barriers *Semicond. Sci. Technol.* **1** 7–27
- [33] Sermage B, Essa Z, Taleb N, Quillec M, Aubin J, Hartmann J M and Veillerot M 2016 Electrochemical capacitance voltage measurements in highly doped silicon and silicon-germanium alloys *J. Appl. Phys.* **119** 155703
- [34] Komatsu Y, Harata D, Schuring E W, Vlooswijk A H G, Katori S, Fujita S, Venema P R and Cesar I 2013 Calibration of electrochemical capacitance-voltage method on pyramid texture surface using scanning electron microscopy *Energy Procedia* **38** 94–100
- [35] Allen F G and Gobeli G W 1962 Work function, photoelectric threshold, and surface states of atomically clean silicon *Phys. Rev.* **127** 150–8